



Research Article

Synthesis and Characterization of Nano Active Filler of Pumice Particle Produced by Sol-Gel Process with Different Precipitation Temperatures for Enhancing the Impact Properties of GFRP Composite

Kuncoro Diharjo*, Andry Rakhman and Wijang Wisnu Raharjo

Mechanical Engineering Department, Engineering Faculty, Sebelas Maret University, Surakarta, Indonesia

Venty Suryanti

Department of Chemistry, Faculty of Mathematics and Natural Sciences, Sebelas Maret University, Surakarta, Indonesia

Sunarto Kaleg

Research Center for Transportation Technology, National Research and Innovation Agency, Bandung, Indonesia

* Corresponding author. E-mail: kuncorodiharjo@ft.uns.ac.id

DOI: 10.14416/j.asep.2025.05.007

Received: 23 October 2024; Revised: 12 December 2024; Accepted: 24 March 2025; Published online: 26 May 2025

© 2025 King Mongkut's University of Technology North Bangkok. All Rights Reserved.

Abstract

Pumice, a volcanic mineral abundant in Indonesia that can contain up to 70% silica, is a great source of nanosilica material. The mesoporous amorphous nanosilica, called nano active filler of pumice particle (nAFPP), has been successfully synthesized using a sol-gel process with different precipitation temperatures at 45, 55, and 65 °C. The nAFPP was characterized using SEM-EDX, Multi-Point BET, and BJH techniques for surface properties and morphologies studies, FTIR for chemical bond studies, XRD for crystallinity properties, and TGA/DTA characterization for thermal stability studies. The influence of nanosilica filler in forming GFRP/nAFPP composites was evaluated using impact testing and morphological analysis with SEM on the fracture surfaces. The result shows that the nanosilica of nAFPP has good purity (93.68%), mesoporous amorphous, nano-sized silica particles, and a pore diameter of 4.36–6.97 nm. The spectra of FTIR display the absorption peaks of the functional group silanol (Si-O-Si). The GFRP/nAFPP composites have higher impact strength than those with pumice particles or without particles. The highest impact strength (97.37 KJ/m²) is achieved in the GFRP composite with 2.5 of nAFPP, and its addition until 10 decreases the impact strength slightly. Further research on this material is needed to accelerate its application.

Keywords: Characterization, GFRP Composite, Impact strength, Nanosilica, Pumice, Synthesis

1 Introduction

Approximately thirty percent of active volcanoes on Earth are located in Indonesia, making it the country with the most active volcanoes [1]. Pumice is a natural mineral originating from a volcano formed by the volcanic gases and materials rapidly cooling [2]. Pumice has been utilized as a raw material in several industries, serving as a low-cost filter material, adsorbing material of pollutants, reinforcement filler, and cement production additive [3]. The pumice is

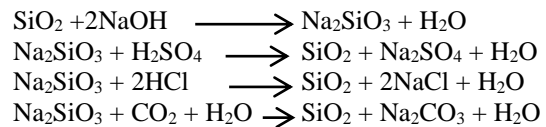
composed of chemical compounds in the form of oxide minerals such as SiO₂, Al₂O₃, Fe₂O₃, K₂O, CaO, Na₂O, TiO₂, and MgO [4]. The composition of pumice compounds mostly contains 70.21% SiO₂ and 13.63% Al₂O₃ [5]. The high silica content in natural pumice is promising as an alternative silica source for various applications. Choosing the right materials is essential for successful and sustainable engineering design. Their mechanical, physical, and chemical properties must meet client expectations [6].

There are many benefits of the nanosilica application on polymer composite, such as reducing matrix failure and improving the mechanical properties, lifespan, heat resistance, and thermal stability without significant degradation [7]–[11]. The uniform dispersion of nanosilica in the matrix can increase the contact between the reinforcement and matrix, thereby improving the thermal and overall mechanical properties. The nanosilica interaction in Glass Fiber Reinforced Polymer (GFRP) composite binds each other through van der Waals interactions and hydrogen bonds, which can increase interfacial strength and transfer mechanical loads more effectively. Nanosilica, which is chemically inert under most conditions, makes it resistant to chemical reactions and corrosion. However, it can be reactive under certain extreme conditions or in the presence of strong acids or bases [12]–[14]. Surface functionalization of nanosilica can enhance its chemical stability and compatibility with different matrixes or environments [10]. The addition of nanosilica can also increase barrier properties against water and gas penetration, as well as an enhancing of fire resistance [14].

Incorporating different nanomaterials is an efficient way to enhance the impact performance of polymer composite [15]. Because of improving the impact performance, engineers have recently preferred hybrid composites of fiber and filler for many applications with high-impact loads, such as propellers, ships, fishing boats, and submarines [16]. Adding hybrid snail shell particles and chicken feather fibers in 3 wt.% on epoxy resin has enhanced its absorbed impact energy from 31.2 to 65.3 joule [17]. In the case of Epoxy – glass fiber composite, adding nanosilica can reduce the fiber failure compared to carbon nanotubes. The addition of nanosilica can also increase barrier properties against water and gas penetration, as well as increase resistance to fire [18]. The application of nanosilica combined with other particles can provide more benefits in optimizing the composite properties due to the excellence of each particle. The GFRP composite's tensile modulus significantly increased when 3 wt.% silica and clay nanoparticles were added, as opposed to the empty composite. In particular, the nanosilica and nano-clay GFRP composites showed an increased tensile modulus of 24.84% and 32.52%, respectively [19]. Barbaz-Isfahani *et al.* have demonstrated the maximum flexural stress (46.517 MPa) of the abaca/polypropylene composites containing 6 wt.% of

halloysite clay nanotubes (HNTs) due to the HNTs' inability to aggregate in the composite's matrix [15].

The parameters of synthesis, including such as temperature, time of precipitation, pH, surfactant, and washing and drying techniques, affect the resulting silica characteristics [20]. Precipitated silica is silica made from the precipitation reaction of silica salt solution (Na_2SiO_3) [21]. The silica salt is then reacted with a mineral acid to precipitate the silica from the salt [22]. Silica precipitation can be made by dissolving many types of organic and inorganic materials containing rich silica, such as rice husk ash, bagasse, palm mill, fly ash, and pumice rock as silica sources [4], [23], [24]. The pumice can be easily extracted after dissolving on sodium hydroxide (NaOH) at 100 °C to produce Na_2SiO_3 . It could be precipitated to produce pure silica (SiO_2) after reacting with a strong mineral acid such as Chloride Acid (HCl), Nitric Acid (HNO_3), or Sulfuric Acid (H_2SO_4). The reaction of silica production from the precipitation process can be assigned as [4]:



Synthetic amorphous silica has very wide applications in various fields, especially mesoporous type silica because the pores in silica can be arranged [25]. The properties of mesoporous or crystalline silica depend on the temperature, reaction conditions, and manufacturing technique in the production process [26], [27]. Mesoporous silica has been widely used as a filler in composite industries, such as in the tire and other rubber industries [24], [28], [29].

When amorphous silica is extracted using temperature and calcination time parameters, the proportion of SiO_2 rises while other oxides and impurities decrease [30]. The combination of acid treatment and HCl calcination produced amorphous nanosilica with a diameter of 45.5 nm and a narrow particle size distribution [31]. Utilizing a modified sol-gel process, palm kernel shell ash was converted into amorphous silica nanoparticles with a silica yield of 54.35% [32].

According to previous studies, adding filler, including aluminum trihydroxide (ATH), graphite, silica, nanoclay, snail powder, and nAFPP, improves the mechanical properties and inhibits flames, respectively [13], [33]–[36]. With its enormous

surface area and mesoporous structure, nanostructured pumice is a great natural thermally stable material that shows promise for several industrial, commercial, and nanotechnology applications, including geopolymers and purifying water [37].

Pumice particles (PP) were synthesized in this research for producing nAFPP with the sol-gel process varied in different precipitation temperatures. Many related studies have been carried out in the sol-gel technique for silica synthesis [38]–[40], but there is limited research using the precipitation temperature parameter and no research applying the precipitation temperature of more than 60 °C [41]. Furthermore, the improvement of polymer composites with nanosilica has been studied by many researchers [7]–[11]. Hopefully, applying pumice-based nanosilica (nAFPP), produced from pumice with a sol-gel method at a precipitated temperature of 65 °C, can give more benefits in enhancing the impact properties of GFRP composite due to the excellent properties of nAFPP. Apart from that, enhancing the impact qualities of GFRP composites by including particles has potential for recent and future applications.

2 Materials and Method

2.1 Materials

Rinjani Mountain on Lombok Island, Indonesia, provided the pumice for producing PP and nAFPP fillers. The matrix was Unsaturated Polyester Resin (UPR) type 268 BQTN branded by Singapore Highpolymer Chemical Products (SHCP), and Methyl Ethyl Ketone Peroxide (MEKP) was applied as cross-linker for 1 from UPR. The chemicals were supplied by PT. Justus Kimia Raya, Indonesia. The Makmur Fantawijaya Chemical Industries, Indonesia, delivered glass fibers Woven Roving Mats (WRM) and Chopped Strand Mats (CSM), which have a weight-to-area ratio of 200 gr/m².

The extraction and precipitation processes of pumice were conducted using analytical chemicals HCl, NaOH, and HNO₃, with concentrations of 37%, 99%, and 65%, respectively. Merck provided all of the chemical reagents with the greatest purity. Ethanol,

NaOH, and distilled water were obtained at the local market.

2.2 Manufacturing of PP

To remove any sticking contaminants, the pumice was first cleaned with purified water and then dried for 12 h at 100 °C. Furthermore, the pumice was processed using a crusher machine to produce PP. Following a 200 mesh ($\leq 74 \mu\text{m}$) filter, PP was cleaned and thermally activated for one hour at 680 °C, with the heating rate at 3.6 degrees/minute. These processes produced the activated PP, and it was further synthesized into nAFPP. All processes are depicted in Figures 1 and 2.

2.3 Manufacturing of nAFPP

The sol-gel process with different precipitation temperatures was utilized to synthesize the silica-rich PP for producing the nAFPP, as illustrated in Figure 2. After dissolving 100 g of PP in 1000 mL of 2.5 M HCl, they were mixed using a stirring machine at 300 rpm and 90 °C for 2 h. The silica-rich PP was separated from the solution by filtering it. The distilled water was used to wash the solution until pH 7, and the particles were separated and dried in an oven at 100 °C for 2 h. Then, the solubilization of 10 g of silica-rich PP in 2 M NaOH solution was conducted at 95 °C for two hours using the stirring machine at 300 rpm. The impurities and residue were then separated by filtering the solution [42]. Furthermore, silica gel was obtained by filtering the fluid after being precipitated in 10 mL of ethanol dispersant and 5 M HNO₃ sufficiently by maintaining it at pH 7 with different variation temperatures of 45, 55, and 65 °C. The precipitation process was carried out using the stirring machine at 300 rpm for 30 min. After being cleaned of contaminants, including sodium, using hot distilled water, the silica gel product was filtered. A vacuum filter with Whatman filter paper no. 41 was used for all filtering procedures, and the dry nAFPP was obtained after the drying process in an oven at 80 °C for 2 h [13]. Herein, sol-gel precipitation methods are used to manufacture nAFPP in the form of amorphous silica successfully.

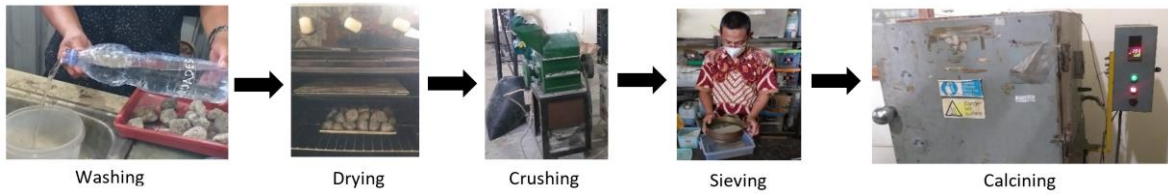


Figure 1: Manufacturing process of activated PP from pumice.

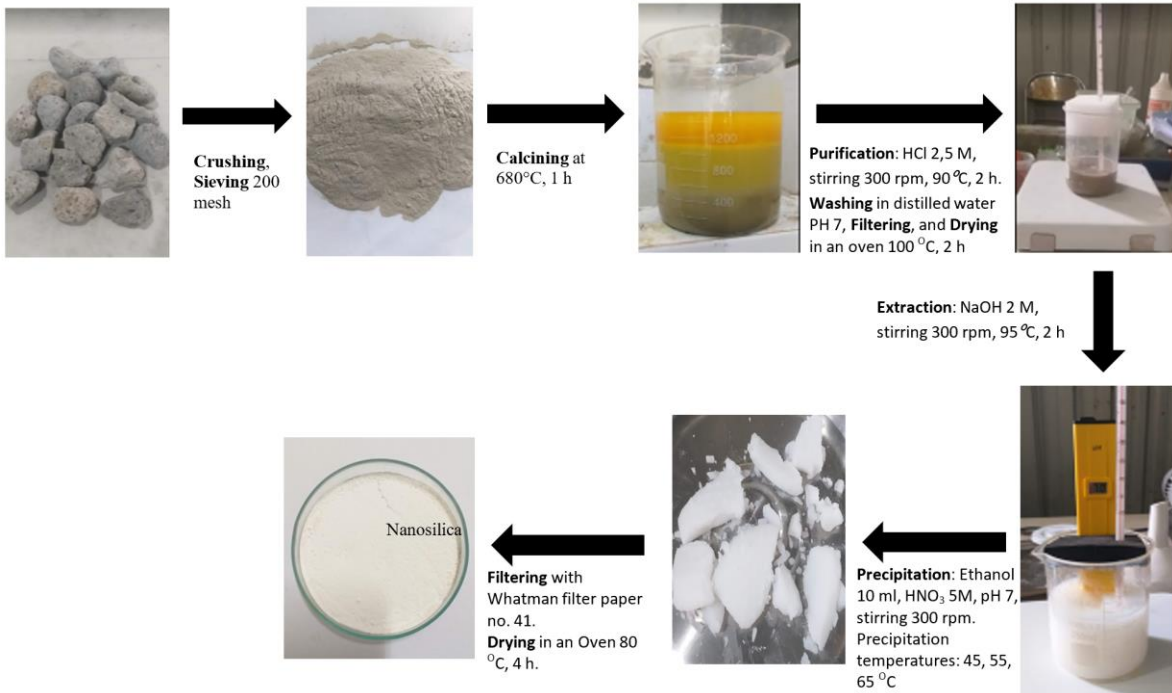


Figure 2: Manufacturing processes of nAFPP from pumice.

2.4 Manufacturing of composites

The activated PP and nAFPP were used in the manufacturing of GFRP composites. The press mold and hand layup techniques were combined to produce the composites. Following Table 1, UPR was first combined with fillers (PP or nAFPP), and the mixture underwent stirring at 3000 rpm for five minutes. It was then kept up until the air bubbles disappeared [43]. The MEKP hardener of 1% by UPR weight was added to the mixture (UPR+filler), and its mixing was conducted in five minutes for homogenous assurance. The CSM and WRM of glass fibers were cut according to the size of a prepared glass molding (300 x 200 x 3; mm). After the CSM-WRM-CSM laminates configuration was arranged on the molding, the matrix (filler/UPR/MEKP) was poured into the molding, and

the cover glass was placed on the mold surface with pressure. After 24 h, the composites were removed from the mold and post-cured in an oven at 100 °C for 60 min [44]. The PP/GFRP and nAFPP/GFRP composites were cut to produce the specimens for izod impact testing according to ASTM D 5941 [45].

Table 1: Specimens of GFRP/PP and GFRP/nAFPP composites.

No	Glass Fibers		Matrix UPR, wt. %	Composites: GFRP/PP	
	Configuration	wt. %		PP content, wt. %	nAFPP content, wt. %
C0			80	0	0
C1	3 laminates:		77.5	2.5	2.5
C2	CSM-WRM-	20	75	5	5
C3	CSM		72.5	7.5	7.5
C4			70	10	10

2.5 Characterization

In this study, the nano-sized nAFPP was characterized using Scanning Electron Microscope – Energy Dispersive X-Ray Spectroscopy (SEM-EDX) brand JEOL JSM-5800LV, Japan, to observe the physical morphology and analyze the elemental of nAFPP. Furthermore, the particle size of nAFPP was also analyzed using Zeta Potential and Particle Size Analyzer, Litesizer 500. The Fourier Transform Infrared Spectroscopy (FTIR) characterization of the nAFPP with Vertex 70, Bruker, USA, was applied to determine the product's chemical linkages. The nAFPP with a precipitated temperature of 65 °C was also evaluated using X-ray diffractometers (XRD) D8 Advance (Bruker) Bragg-Bentano Diffraction Measurement of the N₂ adsorption/desorption isotherm of nAFPP for determining the pore diameter, pore volume, and specific surface area was taken utilizing the Surface Area Analysis Quantachrome (Nova 4200e). Finally, the specific surface area was determined with the Multi-Point BET method, whereas the average pore size and total pore volume were determined using the Barrett, Joyner, and Halenda (BJH) technique [5]. The Thermogravimetric Analysis –Derivative Thermogravimetry (TGA-DTG) was performed on STA PT 1600 (TG-DSC) equipment to evaluate the thermal stability of nAFPP.

2.6 Impact testing

Izod impact apparatus was utilized to investigate the effect of activated-PP and nAFPP on the impact performance of GFRP composites. The impact properties of GFRP/PP and GFRP/nAFPP composites were analyzed and compared to those without filler. The testing was conducted using the TOYOSEIKI - Izod Impact Test equipment at the Central Laboratory, Sebelas Maret University, Indonesia. The specimen position during the testing process and the TOYOSEIKI - Izod Impact Test equipment are shown in Figure 3, following ASTM D 5941 - 96 standards for non-notched specimens [45]. The size of the specimens is 13-mm in width (b), 3-mm in thickness (h), and 65-mm in length. The ASTM standard and the TOYOSEIKI-Izod Impact Test equipment manual book are followed when conducting the testing procedures.

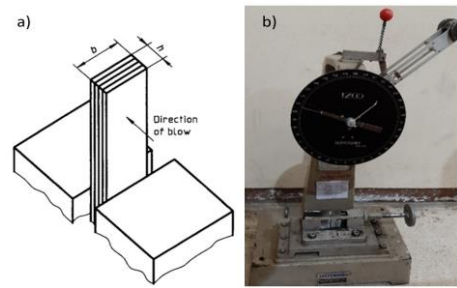


Figure 3: (a) Specimen clamping, (b) Izod impact tester.

3 Results and Discussion

3.1 Characterization of nAFPP

Figure 4 and Table 2 show the morphology and particle size synthesized in this experiment. The silica nanoparticles of nAFPP, which have the sizes of 119_{-44}^{+34} , 73_{-36}^{+20} , and 30_{-8}^{+14} nm (Figure 5 and Table 2) produced by the sol-gel technique with precipitation temperatures of 45, 55, and 65 °C, respectively. The decrease in particle size is inversely proportional to the increase in precipitation temperatures (Figure 5). This outcome is brought about by the dispersant adhering to the particles' surface and creating a shielding layer of macromolecules. This macromolecular shielding layer will stop particle growth to achieve smaller particle sizes and improved dispersibility. Consequently, the sol-gel precipitation technique yields an excellent particle size distribution and allows for the control of particle size through the use of dispersants [46]–[48]. In this study, the dispersant used is ethanol, and the precipitation process's temperature will affect the speed of diffusional mass transfer from ethanol dissolved in water to the surface of the silica particles that were created. The enhancement in temperature increases the diffusivity of ethanol in water so that the speed of ethanol adsorption to silica particles increases and the growth of silica particles is inhibited. The nAFPP sizes in this research are more excellent compared to those that resulted in previous research, producing nanosilica with a size of more than 290 nm [39]. The resulting nAFPP with a size of 30_{-8}^{+14} nm (22–44 nm), is proportional to the size of mesoporous silica nanoparticles (20–50 nm) having a well-ordered hexagonal mesostructure, which is produced using a mixture of cationic surfactant as a template and nonionic block copolymer as a suppressant of grain growth [49].

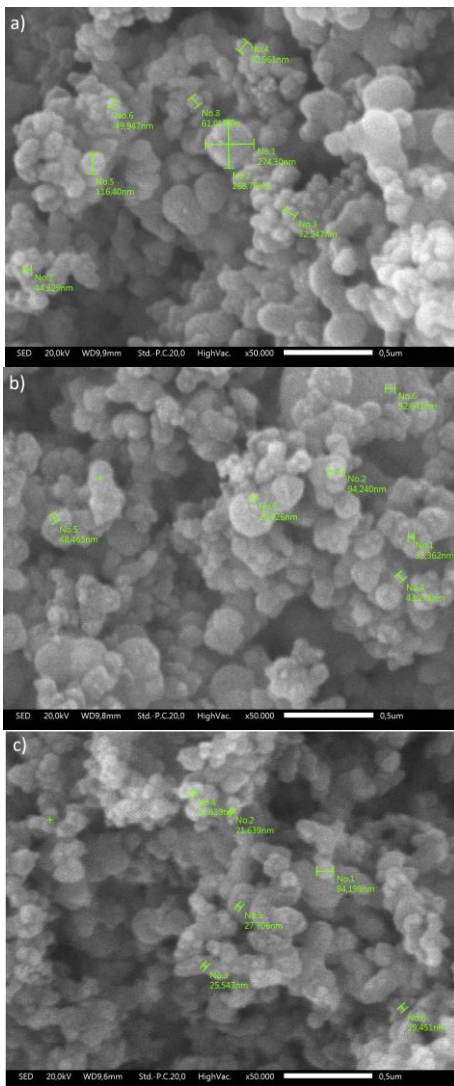


Figure 4: The nAFPP morphology at precipitation temperatures of (a) 45, (b) 55, (c) 65 °C.

Table 2: The nanosilica size of nAFPP.

Pumice Particle	Sodium Silicate	Nitric Acid HNO ₃	Ethanol	Precipitation Temperature	Particle Size
Wt. %	mL	M	mL	°C	nm
10	50	5	10	45	119 ⁺³⁴ ₋₄₄
10	50	5	10	55	73 ⁺²⁰ ₋₃₆
10	50	5	10	65	30 ⁺¹⁴ ₋₈

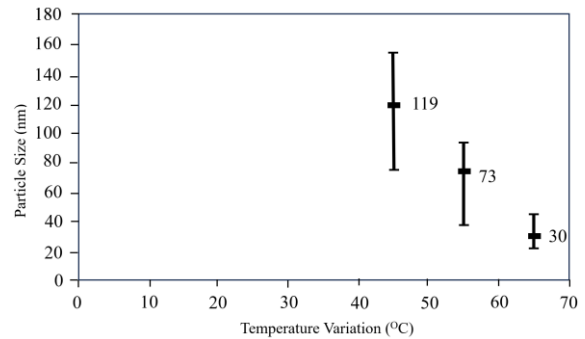


Figure 5: Effect of precipitation temperatures on the size of nAFPP.

In this experiment, the precipitation temperature of 65 °C produces the smallest particle size (30 nm) compared to other precipitation temperatures. The maximum precipitation temperature carried out in this research is 65 °C because the ethanol used as a dispersant will evaporate at 70 °C. Generally, the longer the synthesis time, the greater the reduction in nAFPP concentration because the contact time between reactants takes longer to react and be converted to form nanosilica. Increasing the synthesis temperature and the stirring speed can affect the reduction in reactant concentration, where high temperature and high stirring speed cause the reduction in reactant concentration to be faster, and product formation is also faster. This is because high temperatures can increase the kinetic energy of the reactant particles so that collisions between reacting particles are faster. Then a large stirring speed can increase the frequency of collisions between reactant particles to form nanosilica products [41].

In the future, this sol-gel method can be developed to produce more excellent nanosilica. The most important point of the synthesis of nanosilica was the determining of the initial temperature in the precipitation process, which must be precise to produce the appropriate precipitation temperature. This step is the most difficult level in this study because the volume and type of dispersant can affect the resulting precipitation temperature. For producing nanosilica particles on a commercial scale, providing high-precision production equipment, temperature control equipment, a high level of safety, and a disciplined workforce are important requirements that must be met.

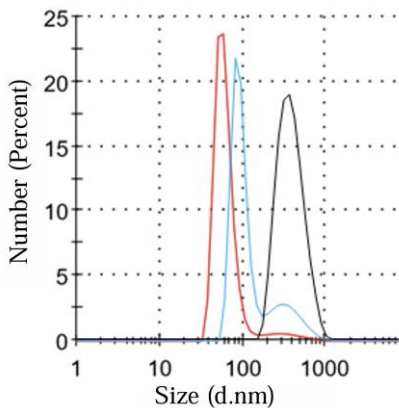


Figure 6: PSA characterization of nAFPP based on size distribution by number.

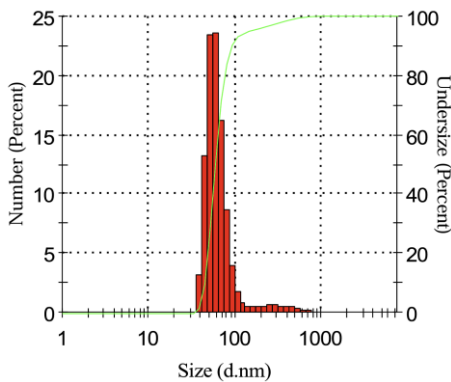


Figure 7: PSA characterization of nAFPP synthesized at precipitation temperature 65 °C based on size distribution by number.

Figure 6 shows the Particle Size Analysis (PSA) of nAFPP synthesized with different precipitation temperatures. The precipitation temperature variations produce changes in the particle sizes of nAFPP. According to Figure 7, the number of nAFPP size distributions at the precipitation temperature of 65 °C is 10% under 43.9 nm, 50% under 58.3 nm, and 90% under 90.9 nm, and the smallest particle size is between 30–40 nm. Using a similar analysis from the SAA test result, the nAFPP treated with 55 °C has size distributions of 10% under 68.3 nm, 50% under 93.4 nm, and 90% under 325 nm, and the smallest size between 40–50 nm. The nAFPP treated with 45 °C has sizes more than 100 nm, and its distribution is 10% under 222 nm, 50% under 342 nm, and 90% under 568 nm. The trend of particle size with PSA (Figure 6 and Figure 7) has the same characteristics as the result of SEM images (Figure 4 and Table 2), whereas they use

different measurement methods. SEM measures by utilizing the optical properties of electrons, while PSA quantifies using the optical properties of light. Thus, the particle size measurement in further research is more suitable using PSA, and SEM is still needed to provide visual evidence. This finding suggests that dispersants can be utilized to manage the distribution and size of the particles produced during the process of the sol-gel technique [46]. Future research could be focussed on gradually increasing the precipitation temperature above 65 °C, exploring alternative dispersants with tailored temperature ranges, and designing laboratory-scale equipment to enhance nanomaterial production and advance.

The precipitation temperature during nAFPP synthesis can influence the mesoporous structure by affecting nucleation, growth kinetics, and particle aggregation. At higher precipitation temperatures, the nucleation rate tends to increase and leads to the formation of smaller particles. These smaller particles can aggregate to form larger structures in a wider surface area and make more mesoporous particles. Lower precipitation temperatures will result in slower nucleation and growth rates, forming larger particles. This can result in a wider pore size and fewer mesopores [22], [50].

The EDX spectrum of the synthesized nAFPP in Figure 8 has peaks of Si, O, and Al. The presence of Si and O confirms the yield of nanosilica from PP. It demonstrates that nanosilica purity can reach 93.68% and the contaminant of aluminum oxide content of 6.32%. Following the calcination and purifying procedures, the presence of Si significantly rose while the existence of Al declined. This outcome shows that silica's carbon is eliminated by calcination, while alkali metals are eliminated by HCl-based treatment. This result can be achieved because acids cannot dissolve silica and are unaffected when the remaining alkali metals, including Fe and Al, dissolve in aqueous solutions.

However, aluminum elemental contaminants were still detected predominantly, as shown by the Al-peak in Figure 8. This could be caused by the incomplete purification process, which could not completely remove all contaminants, including Al. The dominant presence of Al contaminants occurs because the purified particles are pumice powder on a micron scale. This result may change better when the purification process of the pumice is used in nano-size particles, which could minimize existing contaminants, as Mourhly did [3].

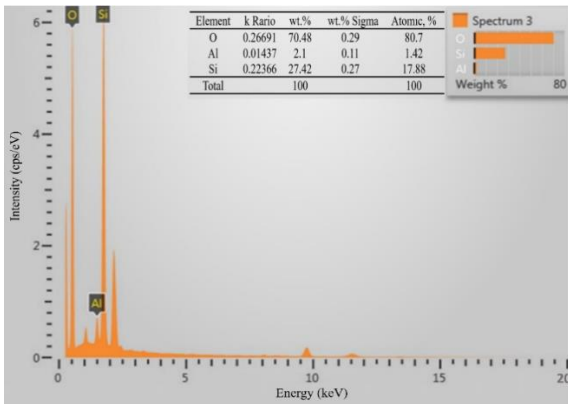


Figure 8: EDX spectrum of nAFPP at a precipitation temperature of 65 °C.

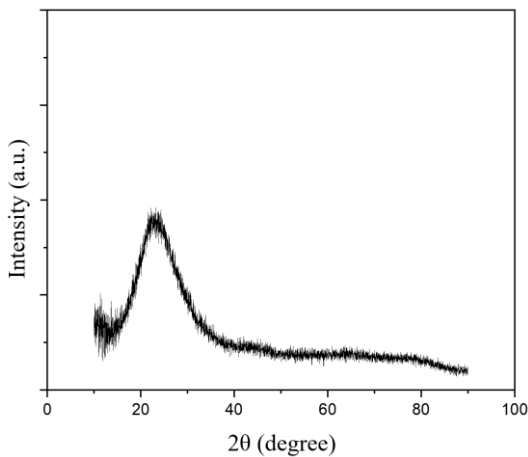


Figure 9: X-ray diffractograms of nAFPP at a precipitation temperature of 65 °C.

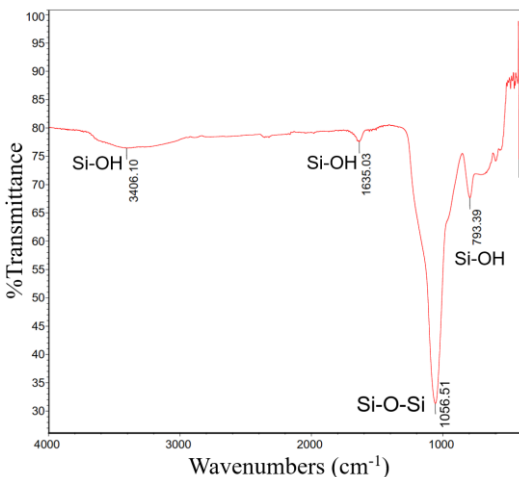


Figure 10: FTIR spectra of nAFPP at a precipitation temperature of 65 °C.

Figure 9 shows the XRD patterns of nAFPP; where the nanoparticles are produced after dissolving 10 wt.% silica-rich pumice particles. This result shows that the nanosilica from the sol-gel precipitation process is amorphous. A sol-gel synthesis process on precipitated silica produces silica with very low crystallinity because of the insufficient active energy for the phase change of silica to quartz. The non-appearance of other peaks in the XRD result indicates that the silica in nAFPP is quite pure without the presence of additional impurity crystals [42]. The temperature and silica processing techniques have a direct impact on the forming of crystalline or amorphous silica [27].

FTIR was utilized to analyze the major chemical group on pure silica particles after precipitation. FTIR spectra of the nano silica-nAFPP were already synthesized, and the result of FTIR spectra is depicted in Figure 10. It shows that the silica has high-purity properties, and Figure 8 shows no organic matter was detected in the nAFPP. A peak of 1056.51 cm^{-1} was associated with symmetric stretching vibration of Si-O in siloxane Si-O-Si, including the peak of 793.39 cm^{-1} . The points of 1635.03 and 3406.10 cm^{-1} indicate bending vibration of -OH from Si-OH and stretching vibrations of -OH from Si-OH, respectively [51], [52].

Table 3: Pore evaluation of nAFPP using SAA.

Presipitation Temperature °C	Surface Area (Multi-Point BET) m^2/g	Average Pore Size (BET) nm	Micropore Volume (HK Method) cc/g	Pore Volume (BJH Desorption) cc/g
45	44.12	6.971	0.015	0.136
55	91.60	4.592	0.032	0.176
65	130.76	4.360	0.053	0.248

The increasing precipitating temperature enhances the kinetic energy [41], and it makes an increase in specific surface area, reduction in average pore size, an increase in specific micropore volume, and an increase in specific pore volume, as shown in Table 3. The sol-gel process, treated with precipitation temperatures of 45, 55, and 65 °C, produces nAFPP with a specific surface area of 44.12, 91.6, and 130.76 m^2/g . Similar to the results of the previous findings by Utama *et al.*, which is 50–140 m^2/g [22]. The treatments also decrease the average pore sizes from 6.971 to 4.360 nm, and the pores may be classified as mesoporous nanosilica with a diameter range between 2 and 50 nm [26]. This nAFPP can be categorized as middle pore volume due to the specific pore volume being between 0.1 and 0.3 cc/g . Although there is a specific micropore volume of 0.015–0.053 cc/g , the

nAFPP has good absorption media, including rubber and polymer, for enhancing the mechanical properties and wear resistance [13], [28], [35].

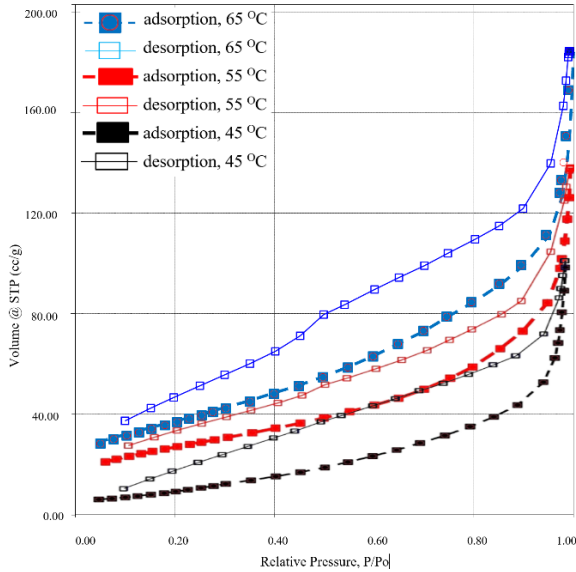


Figure 11: N₂ adsorption/desorption isotherm curve of nAFPP.

According to the IUPAC classification, this adsorption/desorption loop hysteresis, as shown in Figure 11, is similar to the previous findings of PANI-silica nanocomposite electrode material by Zu *et al.*, which has a specific surface area of 81.08 m²/g, with an average pore diameter of 5.72 nm, and total pore volume of 0.20 cc/g [53]. Figure 11 shows that the adsorption isotherm of silica exhibits a characteristic Type IV profile, accompanied by a well-defined H2 hysteresis loop within the relative pressure range of 0.05–1.0 P/P_o.

Furthermore, as observed in Figure 11, all nAFPP samples exhibit a relatively large hysteresis loop size, indicating a substantial amount of adsorbate retained within the pores. Among them, the nAFPP sample precipitated at 65 °C retains the highest amount of adsorbate (N₂) during desorption, suggesting that it possesses the largest number of mesopores. The shape and hysteresis curve are also similar to the isotherm curve of nanosilica synthesized using a microwave, classified as mesoporous nanosilica [52]. It is more adequate for adsorption since this structure can better accommodate large molecules [54].

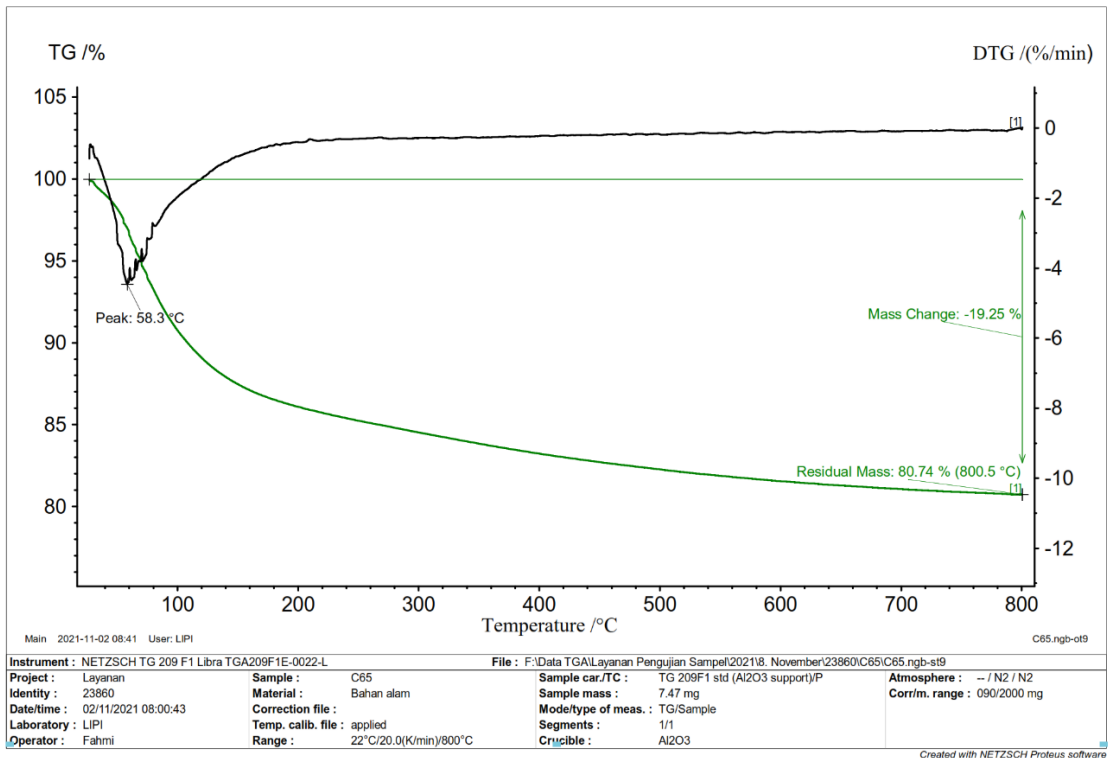


Figure 12: The TGA/DTG of nAFPP.

Figure 12 shows the thermal stability of nAFPP characterized by TGA/DTG. The specific temperature is associated with significant mass loss because the bonded water in mesoporous silica evaporates at the DTG peak of 58.3 °C. The DTG peak at around 58 °C occurred due to the disappearance of water molecules inside the mesoporous silica [55]. Furthermore, the specimen has a significant reduction in mass up to about 200 °C due to the water evaporation being constantly restrained in the mesoporous silica of nAFPP. Further mass loss occurs at 200 to 800 °C because Si-OH bonds condense and become Si-O-Si bonds [56].

3.2 Impact strength of GFRP/ nAFPP composite

All specimens failed to fracture at the pendulum strike line. This fracture mechanism was initiated by the fracture on the front surface, which was subjected to high tensile stress, and this was followed by the breaking of the matrix and fibers. The impact strength of nAFPP/GFRP composites tends to be higher because the nanofiller improves the interaction bond of fiber-matrix, load transfer of fiber-matrix, energy absorption, load distribution, reduction of stress magnitude in certain areas, and energy dissipation mechanisms, such as micro-crack arrest or crack path diversion. The stress distribution in the impact load area is more even due to better interaction between the matrix and fibers [57]–[60].

The result shows that using PP and nAFPP gives an advantage in the impact properties of GFRP composites (Figure 13). Furthermore, the nAFPP/GFRP composite has higher energy absorption and impact strength than the PP/GFRP composite. The highest impact strength 97.37 KJ/m² is achieved on the nAFPP/GFRP composite with 2.5 wt.% nanosilica particles. All GFRP composites with nAFPP have higher impact strength than the similar previous research, with a maximum impact strength of about 92 KJ/m² [61], [62], due to the mesoporous nAFPP having a good absorption with UPR. The use of nAFPP in UPR/GF composite improves interaction bonding with fiber, mechanical properties, failure resistance, and reduction of crack propagation [17] [57]. The nAFPP acts as a link between fibers and matrix to improve the stress transfer from fibers to the matrix and vice versa, as well as make the composite stronger and more rigid [63], [64]. The dispersed nAFPP in the GFRP composite can also reduce the permeability of the composite, and it can act as a

barrier to prevent fractures and make it more resilient [65]. Adding nAFPP makes them more resilient to impact loading-induced deformation and breakage because of the interaction between its constituent compounds, producing more crystallinity [66]. Strong interfacial adhesion between the matrix and fibers may be facilitated by this filler, resulting in a more efficient load transfer mechanism [18], [36]. This can lessen localized stress concentrations by distributing impact loads more uniformly across the composite structure.

However, nAFPP content above 2.5 wt.% reduced the impact strength of the composites. This decrease may be due to filler agglomeration and weak interfacial adhesion between fibers and matrix (UPR/nAFPP), which resulted from inadequate resin content at higher filler loadings [60]. As a result, the stress was distributed unevenly, creating localized stress concentration points that contributed to a decrease in impact strength [67]. Future research should focus on enhancing the mechanical strength of this composite by improving the dispersion of nAFPP, guided by observations of nano-scale particle distribution within the material.

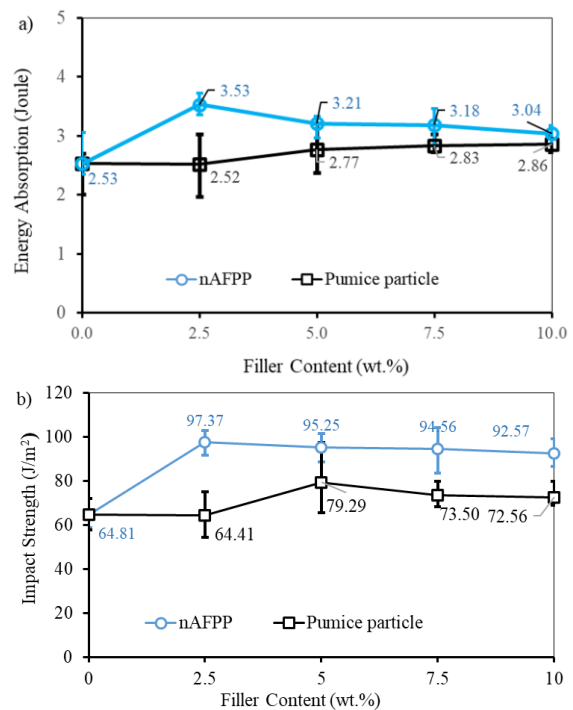


Figure 13: (a) Energy absorption and (b) impact strength of GFRP/PP and GFRP/nAFPP composites.

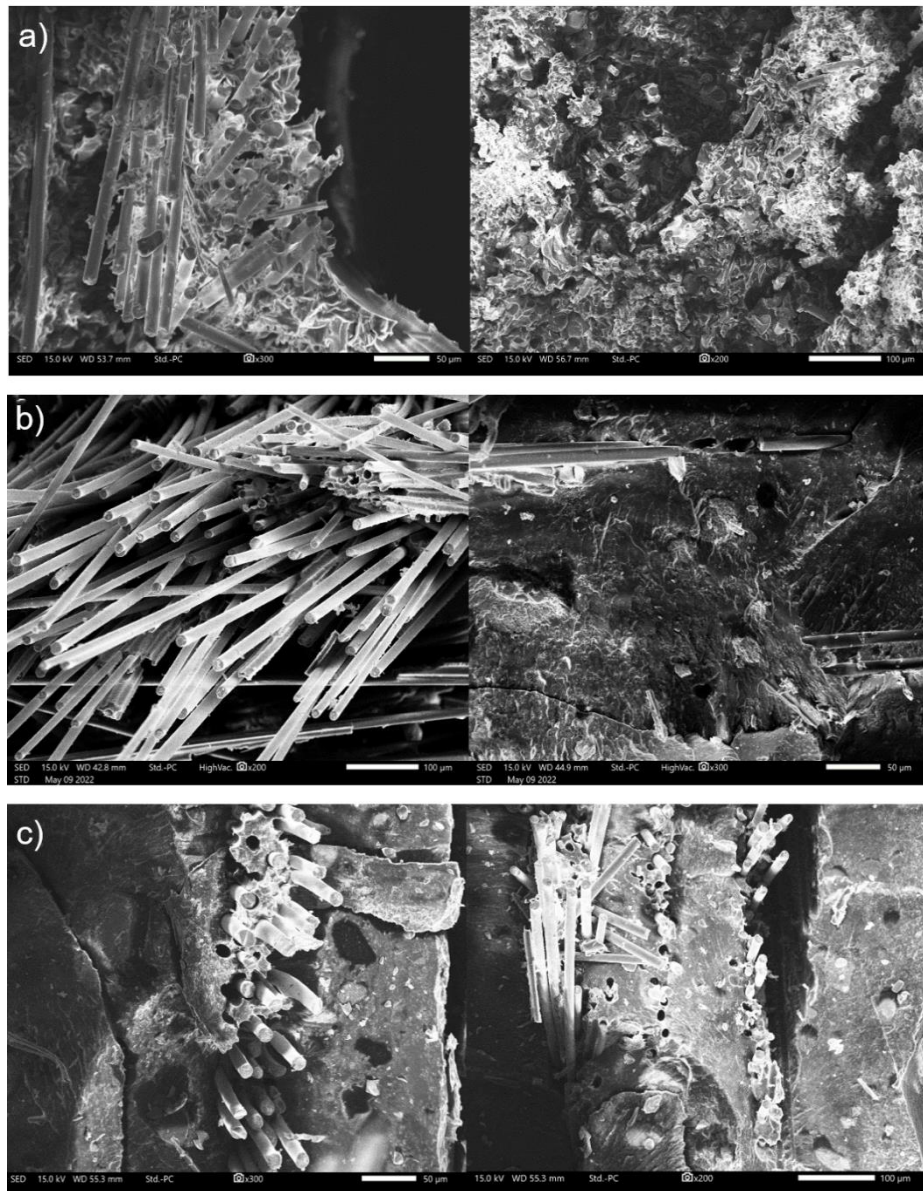


Figure 14: The fracture surface morphology of GFRP/nAFPP composites with nAFPP concentrations of (a) 0 wt.%, (b) 2,5 wt.%, and (c) 5 wt.%.

The fracture surface morphology of the composite with nAFPP of 2.5 wt.% shows no porosity and no crack on the surface of the matrix (Figure 14(b)). It has a good denser matrix to bond the fibers so that the fracture surface of the matrix is not soft-ductile or brittle. For the composite without filler (Figure 14(a)), the pure UPRs matrix also has good bonding with the fiber, as shown by matrix fragments attached to the fibers. Unfortunately, the fracture surface of pure

UPRs matrix is categorized as a soft-ductile characteristic, shown by the rougher fracture surface. This soft-ductile matrix can usually bond with other materials (fiber), but its strength is low, as shown by fiber pullout holes. Another finding is many porosities on the fracture surface of the pure UPR matrix, which may be caused by the presence of air bubbles during the manufacturing process. The soft-ductile matrix can bond with fibers but not evenly over all-fiber surfaces

due to porosity. The nAFPP addition of 5, 7.5, and 10 wt.% decreases the impact strength slightly. The increase of filler content has the potential to form the inhomogeneity of its distribution and the filler agglomeration, producing a barrier of contact between reinforcement and matrix. This excess content of fillers reduces the load transfer capacity and overall mechanical and thermal properties [68].

The failure surface morphology of the composite with 5 wt.% of nAFPP shows a good bonding between matrix and glass fiber, shorter fiber pull-out, high denser matrix, and no void (Figure 14(c)). Unfortunately, the fracture surface is brittle, characterized by a flat fracture surface and a long-wide failure of matrix fracture. Theoretically, the brittle matrix is sensitive to impact loads, so there is a slight decrease in impact strength (Figure 13). However, the composite's higher impact strength with nAFPP than that without nAFPP is caused by the ability of nAFPP to form a bonding network with UPR and fibers in the composite [69]. The failure surfaces of the GFRP/nAFPP/composites show strong interfacial bonding of fiber–matrix. The higher nAFPP content influences an increase of matrix denser, stronger interfacial bonding, and support more loads [70]. However, it can reduce the impact strength of the composite because of the rise of brittleness due to the possibility of agglomeration [60].

Additionally, integrating nAFPP can enhance barrier properties against water and gas penetration while also improving fire resistance [18]. This barrier effect arises from the chemical bonding between functional groups on the nAFPP surface and the glass fiber. Moreover, designing components intended for exposure to high-impact or shock loads should be guided by impact strength evaluations to anticipate potential failures. Future research on impact properties should consider various contributing factors and propose effective strategies to reduce the material's susceptibility to potential weaknesses.

3.3 Market potential and application

According to a report by Research and Markets in 2023, around three million tons of synthetic amorphous silica were produced worldwide in 2016. Between 2022 and 2023, the global market for nanosilica increased from \$3.95 billion to \$4.28

billion. However, the nanosilica price has still prevented its widespread application, and the high potential of agglomeration of nanosilica has led to rising costs. However, as security and maintenance expenses are major considerations, employing nanosilica in marine constructions can offer advantages in terms of value and cost [71].

The GFRP/nAFPP composites, with an impact strength of 92.57–97.37 KJ/m², are recommended for usage in the marine, automotive, and aerospace industries. They have a high chance of receiving impact loads with sea waves and other applications as modular segments to absorb energy in case of a collision [72].

4 Conclusions

The synthesis of nAFPP from PP has been successfully carried out by a sol-gel method with different precipitation temperatures. The increased precipitation temperatures in the synthesis process decrease the nanosilica size. The purity of nanosilica reaches up to 93.68%, and the process can produce mesoporous nanosilica with low crystallinity. The nAFPP nanosilica has a specific surface area of 44.12, –130.76 m²/g, average pore sizes of 4.360–6.971 nm, specific micropore pore of 0.015 – 0.053 cc/g, and specific pore volume of 0.136–0.248 cc/g. Adding PP and nAFPP into GFRP composites increases impact toughness and impact energy absorption. The nAFPP are useful for improving cohesion between fibers and matrix. The highest impact strength (97.37 KJ/m²) is achieved on the GFRP composite with nAFPP of 2.5 wt.%, and the strength decreases slightly along with an increase of nAFPP content. The fracture surfaces of GFRP composites with nAFPP show a more brittle failure. The GFRP/nAFPP composites have a good potential for usage in the marine, automotive, and aerospace industries. Further research supporting the application of this composite is also needed.

Acknowledgments

This research was funded by the Institute for Research and Community Service (LPPM), Sebelas Maret University (UNS), Indonesia, and supported in the characterization by the National Research and Innovation Agency (BRIN), Indonesia.

Author Contributions

A.R., K.D., W.W.R., and V.S.: Conceptualization; A.R., K.D., W.W.R., and V.S.: methodology; A.R., and K.D.: software; K.D., W.W.R., V.S., and S.K.: validation; A.R., K.D., and S.K.: formal analysis; A.R., K.D., and S.K.: investigation; A.R., K.D., and S.K.: resources; A.R. and K.D.: data curation; A.R. and K.D.: writing—original draft preparation; A.R., K.D., and W.W.R.: writing—review and editing; A.R. and K.D.: visualization; K.D., W.W.R., and V.S.: supervision; A.R. and K.D.: project administration; K.D., W.W.R., and V.S.: funding acquisition; A.R., K.D., and W.W.R., are the main contributors of the manuscript. All authors have read and agreed to the published version of the manuscript.

Conflicts of Interest

The authors declare no conflicts of interest.

References

- [1] I. Pratomo, "Klasifikasi gunung api aktif Indonesia, studi kasus dari beberapa letusan gunung api dalam sejarah," *Indonesian Journal on Geoscience*, vol. 1, no. 4, pp. 209–227, Dec. 2006, doi: 10.17014/ijog.1.4.209-227.
- [2] O. Ilter, "Use of pumice in mortar and rendering for lightweight building block," M.S. thesis, Department of Civil Engineering, Eastern Mediterranean University, 2010.
- [3] A. Mourhly, M. Khachani, A. El Hamidi, M. Kacimi, M. Halim, and S. Arsalane, "The synthesis and characterization of low-cost mesoporous silica SiO₂ from local pumice rock," *Nanomaterials and Nanotechnology*, vol. 5, 2015, doi: 10.5772/62033.
- [4] S. Muljani, R. Dewati, Suprihatin, K. Sumada, R. Dewati, Suprihatin, and K. Sumada, "Precipitated silica by precipitation process of the sodium silicate solution with carbon dioxide gas (CO₂) on fixed bed column," in *Nusantara Science and Technology Proceedings*, Galaxy Science, Apr. 2019, pp. 231–236. doi: 10.11594/nstp.2019.0230.
- [5] I. J. Fernandes, D. Calheiro, F. A. L. Sánchez, A. L. D. Camacho, T. L. A. de C. Rocha, C. A. M. Moraes, and V. C. de Sousa, "Characterization of silica produced from rice husk ash: Comparison of purification and processing methods," *Materials Research*, vol. 20, no. suppl 2, pp. 512–518, Oct. 2017, doi: 10.1590/1980-5373-mr-2016-1043.
- [6] M. Palaniappan, S. Palanisamy, T. M. Murugesan, N. H. Alrasheedi, S. Ataya, S. Tadepalli, and A. A. Elfar, "Novel ficus retusa l. aerial root fiber: A sustainable alternative for synthetic fibres in polymer composites reinforcement," *Biomass Conversion and Biorefinery*, vol. 15, no. 5, pp. 7585–7601, Mar. 2025, doi: 10.1007/s13399-024-05495-4.
- [7] H. Li, B. Cheng, W. Gao, C. Feng, C. Huang, Y. Liu, P. Lu, and H. Zhao, "Recent research progress and advanced applications of silica/polymer nanocomposites," *Nanotechnology Reviews*, vol. 11, no. 1, pp. 2928–2964, 2022, doi: 10.1515/ntrev-2022-0484.
- [8] A. Jumahat, C. Soutis, S. A. Abdullah, and S. Kasolang, "Tensile properties of nanosilica/epoxy nanocomposites," *Procedia Engineering*, vol. 41, no. Iris, pp. 1634–1640, 2012, doi: 10.1016/j.proeng.2012.07.361.
- [9] C. M. Manjunatha, A. C. Taylor, A. J. Kinloch, and S. Sprenger, "The tensile fatigue behaviour of a silica nanoparticle-modified glass fibre reinforced epoxy composite," *Composites Science and Technology*, vol. 70, no. 1, pp. 193–199, 2010, doi: 10.1016/j.compscitech.2009.10.012.
- [10] Y. Gitara, R. Barbaz-isfahani, S. Sabersamandari, and M. Sadighi, "Effect of nanoparticles on the improving mechanical behavior of GFRP composites in a corrosive environment," *Journal of Nanoanalysis*, vol. 9, no. 1, pp. 68–82, 2022, doi: 10.22034/jna.2021.1930895.1256.
- [11] G. Tsintskaladze, T. Kordzakhia, R. Skhvitaridze, T. Sharashenidze, M. Zautashvili, and G. Beridze, "Physical and chemical characteristics of pumice from some regions of georgia and the prospects for its use in lightweight concrete with environmental advantages," in *Environmental Technology and Sustainability*. New York: Apple Academic Press, pp. 247–256, 2024. doi: 10.1201/9781003397960-16.
- [12] S. Kamarian, A. Khalvandi, Tran, T. M. Nguyen, Barbaz-Isfahani, Reza, S. Saber-Samandari, and J.-I. Song, "Predicting ESP and HNT effects on the mechanical properties of eco-friendly composites subjected to micro-indentation test," *Advances in Nano Research*, vol. 15, no. 4, pp. 315–328, 2023, doi: 10.12989/anr.2023.15.4.315.
- [13] A. Rakhman, K. Diharjo, W. W. Raharjo, V.

- Suryanti, and S. Kaleg, "Improvement of fire resistance and mechanical properties of glass fiber reinforced plastic (GFRP) composite prepared from combination of active nano filler of modified pumice and commercial active fillers," *Polymers*, vol. 15, no. 1, 2023, doi: 10.3390/polym15010051.
- [14] S. A. O. Adeyeye and T. J. Ashaolu, "Applications of nano-materials in food packaging: A review," *Journal of Food Process Engineering*, vol. 44, no. 7, pp. 1–8, 2021, doi: 10.1111/jfpe.13708.
- [15] R. Barbaz-Isfahani, A. Khalvandi, T. Mai Nguyen Tran, S. Kamarian, S. Saber-Samandari, and J. Song, "Synergistic effects of egg shell powder and halloysite clay nanotubes on the thermal and mechanical properties of abacá/polypropylene composites," *Industrial Crops and Products*, vol. 205, no. May, p. 117498, Dec. 2023, doi: 10.1016/j.indcrop.2023.117498.
- [16] S. O. Okuma, M. Obaseki, D. O. Ofuyekpone, and O. E. Ashibudike, "A review assessment of fiber-reinforced polymers for maritime applications," *Journal of Advanced Industrial Technology and Application*, vol. 4, no. 1, pp. 17–28, 2023, doi: 10.30880/jaita.2023.04.01.003.
- [17] A. D. Akinwekomi, I. O. Oladele, L. N. Onuh, E. E. Essien, N. I. Agbeboh, and M. O. Idris, "Development and characterization of hybrid particulate-fiber reinforced epoxy composites," *Applied Science and Engineering Progress*, vol. 17, no. 4, 2024, Art. no. 7391, doi: 10.14416/j.asep.2024.06.001.
- [18] S. Alimirzaei, R. Barbaz-isfahani, A. Khodaei, and M. Ahmadi, "Investigating the flexural behavior of nanomodified multi-delaminated composites using acoustic emission technique," *Ultrasonics*, vol. 138, 2024, Art. no. 107249, doi: 10.1016/j.ultras.2024.107249.
- [19] F. Rahmani, R. Barbaz-Isfahani, S. Saber-Samandari, and M. Salehi, "Experimental and analytical investigation on forced and free vibration of sandwich structures with reinforced composite faces in an acidic environment," *Heliyon*, vol. 9, no. 10, Oct. 2023, Art. no. e20864, doi: 10.1016/j.heliyon.2023.e20864.
- [20] M. A. Rida, and, and F. Harb, "Synthesis and characterization of amorphous silica nanoparticles from aqueous silicates using cationic surfactants," *Journal of Metals, Materials and Minerals*, vol. 24, no. 1, pp. 37–42, 2014, doi: 10.14456/jmmm.2014.7.
- [21] P. Chindaprasirt and U. Rattanasak, "Eco-production of silica from sugarcane bagasse ash for use as a photochromic pigment filler," *Scientific Reports*, vol. 10, no. 1, p. 9890, Jun. 2020, doi: 10.1038/s41598-020-66885-y.
- [22] P. S. Utama, R. Yamsaengsung, and C. Sangwichien, "Production and characterization of precipitated silica from palm oil mill fly ash using CO₂ impregnation and mechanical fragmentation," *Brazilian Journal of Chemical Engineering*, vol. 36, no. 1, pp. 523–530, 2019, doi: 10.1590/0104-6632.20190361s20170458.
- [23] Y. Zhang, Z. Zeng, H. Qi, X. Yin, H. Li, X. Wang, and S. Chen, "Two-stage influences of hydrothermal fluids on pumice near the Iheya North hydrothermal field, Okinawa Trough," *Marine Georesources & Geotechnology*, vol. 36, no. 4, pp. 393–404, May 2018, doi: 10.1080/1064119X.2017.1318987.
- [24] M. W. Syabani, I. Amaliyana, I. Hermiyati, and Y. I. Supriyatna, "Silica from geothermal waste as reinforcing filler in artificial leather," *Key Engineering Materials*, vol. 849, pp. 78–83, Jun. 2020, doi: 10.4028/www.scientific.net/KEM.849.78.
- [25] N. Pal, J.-H. Lee, and E.-B. Cho, "Recent trends in morphology-controlled synthesis and application of mesoporous silica nanoparticles," *Nanomaterials*, vol. 10, no. 11, p. 2122, Oct. 2020, doi: 10.3390/nano10112122.
- [26] R. Narayan, U. Nayak, A. Raichur, and S. Garg, "Mesoporous silica nanoparticles: A comprehensive review on synthesis and recent advances," *Pharmaceutics*, vol. 10, no. 118, pp. 1–49, Aug. 2018, doi: 10.3390/pharmaceutics10030118.
- [27] I. J. Fernandes, C. A. M. Moraes, J. R. J. Egea, and V. C. Sousa, "Production and characterization of silica materials from rice husk ash by different combustion processes," *Powder Technology*, vol. 436, 2024, doi: 10.1016/j.powtec.2024.119473.
- [28] B. Xue, X. Wang, L. Yu, B. Di, Z. Chen, Y. Zhu, and X. Liu, "Self-assembled lignin-silica hybrid material derived from rice husks as the sustainable reinforcing fillers for natural rubber," *International Journal of Biological Macromolecules*, vol. 145, pp. 410–416, Feb. 2020, doi: 10.1016/j.ijbiomac.2019.12.182.
- [29] S. S. Pole and A. I. Isayev, "The nonlinear stress

- relaxation behavior after a step shear of star-shaped styrene-butadiene rubber filled with precipitated silica: Experiment and simulation,” *Journal of Applied Polymer Science*, vol. 138, no. 12, Mar. 2021, doi: 10.1002/app.50080.
- [30] J. A. Santana Costa and C. M. Paranhos, “Systematic evaluation of amorphous silica production from rice husk ashes,” *Journal of Cleaner Production*, vol. 192, pp. 688–697, Aug. 2018, doi: 10.1016/j.jclepro.2018.05.028.
- [31] L. N. A. Tuan, L. T. K. Dung, L. D. T. Ha, N. Q. Hien, D. V. Phu, and B. D. Du, “Preparation and characterization of nanosilica from rice husk ash by chemical treatment combined with calcination,” *Vietnam Journal of Chemistry*, vol. 55, no. 4, Sep. 2017, doi: 10.15625/2525-2321.2017-00490.
- [32] P. E. Imoisili, K. O. Ukoba, and T.-C. Jen, “Green technology extraction and characterisation of silica nanoparticles from palm kernel shell ash via sol-gel,” *Journal of Materials Research and Technology*, vol. 9, no. 1, pp. 307–313, Jan. 2020, doi: 10.1016/j.jmrt.2019.10.059.
- [33] M. Zainudin, K. Diharjo, M. Kaavessina, and D. Setyanto, “The properties degradation of exposed GFRP roof,” *AIP Conference Proceedings*, vol. 1931, pp. 1–8, 2018, doi: 10.1063/1.5024122.
- [34] B. Mylsamy, S. K. M. Shanmugam, K. Aruchamy, S. Palanisamy, R. Nagarajan, and N. Ayrilmis, “A review on natural fiber composites: polymer matrices, fiber surface treatments, fabrication methods, properties, and applications,” *Polymer Engineering and Science*, vol. 64, no. 6, pp. 2345–2373, Jun. 2024, doi: 10.1002/pen.26713.
- [35] T. P. Sathishkumar, P. Navaneethkrishnan, and P. Maheskumar, “Thermal stability and tribological behaviors of tri-fillers reinforced epoxy hybrid composites,” *Applied Science and Engineering Progress*, vol. 14, no. 4, pp. 727–737, 2021, doi: 10.14416/j.asep.2021.08.002.
- [36] K. Diharjo, F. Gapsari, A. Andoko, M. N. Wijaya, S. Mavinkere Rangappa, and S. Siengchin, “Flammability and thermal resistance of ceiba petandra fiber-reinforced composite with snail powder filler,” *Polymer Composites*, vol. 45, no. 6, pp. 1–14, 2024, doi: 10.1002/pc.28100.
- [37] S. Alraddadi, “The finite size effect on the surface structure and thermal properties of nanostructured natural pumice,” *Advances in Materials and Processing Technologies*, pp. 1–13, Mar. 2023, doi: 10.1080/2374068X.2023.2189673.
- [38] D. Bokov, A. T. Jalil, S. Chupradit, W. Suksatan, M. J. Ansari, I. H. Shewael, G. H. Valiev, and E. Kianfar, “Nanomaterial by sol-gel method: synthesis and application,” *Advances in Materials Science and Engineering*, vol. 2021, no. 1, Jan. 2021, doi: 10.1155/2021/5102014.
- [39] Ł. Klapiszewski, M. Królak, and T. Jesionowski, “Silica synthesis by the sol-gel method and its use in the preparation of multifunctional biocomposites,” *Central European Journal of Chemistry*, vol. 12, no. 2, pp. 173–184, 2014, doi: 10.2478/s11532-013-0370-9.
- [40] L. P. Singh, S. K. Bhattacharyya, R. Kumar, G. Mishra, U. Sharma, G. Singh, and S. Ahalawat, “Sol-gel processing of silica nanoparticles and their applications,” *Advances in Colloid and Interface Science*, vol. 214, pp. 17–37, 2014, doi: 10.1016/j.cis.2014.10.007.
- [41] F. Saputra, A. Fadli, and A. Amri, “Kinetika reaksi pada sintesis hidroksiapatit dengan metode presipitasi,” *Jurnal Online Mahasiswa Fakultas Teknik Universitas Riau*, vol. 3, no. 1, pp. 1–6, 2016.
- [42] U. Zulfiqar, T. Subhani, and S. Wilayat Husain, “Towards tunable size of silica particles from rice husk,” *Journal of Non-Crystalline Solids*, vol. 429, pp. 61–69, 2015, doi: 10.1016/j.jnoncrysol.2015.08.037.
- [43] T. D. Hapuarachchi and T. Peijs, “Aluminium trihydroxide in combination with ammonium polyphosphate as flame retardants for unsaturated polyester resin,” *Express Polymer Letters*, vol. 3, no. 11, pp. 743–751, 2009, doi: 10.3144/expresspolymlett.2009.92.
- [44] K. Diharjo, N. S. Suharty, A. E. B. Nusantara, and R. Afandi, “The effect of sokka clay on the tensile and burning properties of rPP/clay composite,” *Advanced Materials Research*, vol. 1123, pp. 338–342, 2015, doi: 10.4028/www.scientific.net/amr.1123.338.
- [45] *Standard test method for determining the izod impact strength of plastics*, ASTM D5941-96, 1996.
- [46] X. Cai, R. Y. Hong, L. S. Wang, X. Y. Wang, H. Z. Li, Y. Zheng, and D. G. Wei, “Synthesis of silica powders by pressured carbonation,” *Chemical Engineering Journal*, vol. 151, no. 1–3, pp. 380–386, 2009, doi: 10.1016/j.cej.2009.03.060.

- [47] J. Lee, T. Lee, K. Kim, B. Kim, G. Kwag, J. Kim, S. Ji, W. Kim, and H. Paik, "Poly(styrene-*r*-butadiene)-*b*-poly(poly(ethylene glycol) methyl ether methacrylate) as a silica dispersant in rubber compounds," *Polymer International*, vol. 63, no. 5, pp. 908–914, May 2014, doi: 10.1002/pi.4644.
- [48] Z. Zhang, A. E. Berns, S. Willbold, and J. Buitenhuis, "Synthesis of poly(ethylene glycol) (PEG)-grafted colloidal silica particles with improved stability in aqueous solvents," *Journal of Colloid and Interface Science*, vol. 310, no. 2, pp. 446–455, Jun. 2007, doi: 10.1016/j.jcis.2007.02.024.
- [49] K. Suzuki, K. Ikari, and H. Imai, "Synthesis of silica nanoparticles having a well-ordered mesostructure using a double surfactant system," *Journal of the American Chemical Society*, vol. 126, no. 2, pp. 462–463, Jan. 2004, doi: 10.1021/ja038250d.
- [50] A. Mourhly, F. Jhilal, A. E. Hamidi, M. Halim, and S. Arsalane, "Highly efficient production of mesoporous nano-silica from unconventional resource: Process optimization using a central composite design," *Microchemical Journal*, vol. 145, pp. 139–145, 2019, doi: 10.1016/j.microc.2018.10.030.
- [51] A. F. Lourenço, J. A. F. Gamelas, and P. J. Ferreira, "Increase of the filler content in papermaking by using a silica-coated PCC filler," *Nordic Pulp and Paper Research Journal*, vol. 29, no. 2, pp. 240–245, May 2014, doi: 10.3183/npprj-2014-29-02-p240-245.
- [52] B. Kurc, "Precipitated silica as filler for polymer electrolyte based on poly(acrylonitrile)/sulfolane," *Journal of Solid State Electrochemistry*, vol. 18, no. 7, pp. 2035–2046, Jul. 2014, doi: 10.1007/s10008-014-2451-x.
- [53] L. Zu, X. Cui, Y. Jiang, Z. Hu, H. Lian, Y. Liu, Y. Jin, Y. Li, and X. Wang, "Preparation and electrochemical characterization of mesoporous polyaniline-silica nanocomposites as an electrode material for pseudocapacitors," *Materials*, vol. 8, no. 4, pp. 1369–1383, Mar. 2015, doi: 10.3390/ma8041369.
- [54] E. C. Peres, J. C. Slaviero, A. M. Cunha, A. Hosseini-Bandegharai, and G. L. Dotto, "Microwave synthesis of silica nanoparticles and its application for methylene blue adsorption," *Journal of Environmental Chemical Engineering*, vol. 6, no. 1, pp. 649–659, 2018, doi: 10.1016/j.jece.2017.12.062.
- [55] C. J. G. V. D. Grift, P. A. Elberse, A. Mulder, and J. W. Geus, "Preparation of silica-supported copper catalysts by means of deposition-precipitation," *Applied Catalysis*, vol. 59, no. 1, pp. 275–289, Mar. 1990, doi: 10.1016/S0166-9834(00)82204-6.
- [56] A. Lazaro, Y. X. Chen, C. Verhoeven, and Y. Hendrix, "One-step synthesis of ordered mesoporous silica from olivine and its pore size tailoring," *Journal of Cleaner Production*, vol. 238, Nov. 2019, Art. no. 117951, doi: 10.1016/j.jclepro.2019.117951.
- [57] K. Aruchamy, M. Karuppusamy, S. Krishnakumar, S. Palanisamy, M. Jayamani, K. Sureshkumar, S. K. Ali, and S. A. Al-Farraj, "Enhancement of mechanical properties of hybrid polymer composites using palmyra palm and coconut sheath fibers: The role of tamarind shell powder," *BioResources*, vol. 20, no. 1, pp. 698–724, Nov. 2024, doi: 10.15376/biores.20.1.698-724.
- [58] T. Raja and Y. Devarajan, "Study on the mechanical and thermal properties of basalt fiber-reinforced lead oxide nanoparticle polymer composite for advanced energy storage applications," *Journal of Energy Storage*, vol. 108, Feb. 2025, Art. no. 115079, doi: 10.1016/j.est.2024.115079.
- [59] D. A. Durressa, E. G. Koricho, A. N. Ali, and G. A. Kebede, "Characterization and modeling of residual elastic properties of impact damaged glass fiber composite," *Results in Engineering*, vol. 25, p. 103721, Mar. 2025, doi: 10.1016/j.rineng.2024.103721.
- [60] R. Ramasubbu, A. Kayambu, S. Palanisamy, and N. Ayrilmis, "Mechanical properties of epoxy composites reinforced with *Areca catechu* fibers containing silicon carbide," *BioResources*, vol. 19, no. 2, pp. 2353–2370, Feb. 2024, doi: 10.15376/biores.19.2.2353-2370.
- [61] T. Wibawa, K. Diharjo, D. Ariawan, W. W. Raharjo, C. H. Wibowo, F. N. Saputro, A. Rakhman, A. Muharam, S. Kaleg, A. Hapid, and M. Zulkefly, "Enhancing the mechanical and fire-resistant properties of GFRP composite using boric acid and sodium silicate fillers," *Engineering, Technology and Applied Science Research*, vol. 14, no. 6, pp. 18911–18922, 2024, doi: 10.48084/etasr.9271.
- [62] K. Sravanthi, V. Mahesh, and B. Nageswara

- Rao, "Influence of micro and nano carbon fillers on impact behavior of GFRP composite materials," *Materials Today: Proceedings*, vol. 37, pp. 1075–1078, 2021, doi: 10.1016/j.matpr.2020.06.298.
- [63] S. Y. Fu, X. Q. Feng, B. Lauke, and Y. W. Mai, "Effects of particle size, particle/matrix interface adhesion and particle loading on mechanical properties of particulate-polymer composites," *Composites Part B: Engineering*, vol. 39, no. 6, pp. 933–961, 2008, doi: 10.1016/j.compositesb.2008.01.002.
- [64] I. Erunkulu, G. Malumbela, and O. P. Oladijo, "Geopolymer synthesis and alkaline activation technique of fly ash and slag source material: a review," *Applied Science and Engineering Progress*, vol. 16, no. 3, Jan. 2022, Art. no. 6600, doi: 10.14416/j.asep.2023.01.005.
- [65] T. Nanda, K. Singh, D. Shelly, and R. Mehta, "Advancements in multi-scale filler reinforced epoxy nanocomposites for improved impact strength: a review," *Critical Reviews in Solid State and Materials Sciences*, vol. 46, no. 4, pp. 281–329, 2021, doi: DOI: 10.1080/10408436.2020.1777934.
- [66] N. S. Suharty, H. Ismail, K. Diharjo, M. Nizam, and M. Firdaus, "Improvement of inflammability and biodegradability of bio-composites using recycled polypropylene with kenaf fiber containing mixture fire retardant," *Advanced Materials Research*, vol. 950, pp. 18–23, Jun. 2014, doi: 10.4028/www.scientific.net/AMR.950.18.
- [67] A. Kar, D. Saikia, S. Palanisamy, and N. Pandiarajan, "Effect of fiber loading on the mechanical, morphological, and dynamic mechanical characteristics of *calamus tenuis* fiber reinforced epoxy composites," *Journal of Vinyl and Additive Technology*, vol. 31, no.1, pp. 1–17, 2024, doi: 10.1002/vnl.22167.
- [68] S. Kaleg, D. Ariawan, and K. Diharjo, "The flexural strength of glass fiber reinforced polyester filled with aluminum tri-hydroxide and montmorillonite," *Key Engineering Materials*, vol. 772, pp. 28–32, 2018, doi: 10.4028/www.scientific.net/KEM.772.28.
- [69] F. A. dos Santos, G. C. V. Iulianelli, and M. I. B. Tavares, "The use of cellulose nanofillers in obtaining polymer nanocomposites: Properties, processing, and applications," *Materials Sciences and Applications*, vol. 07, no. 05, pp. 257–294, 2016, doi: 10.4236/msa.2016.75026.
- [70] G. V. Prasad, S. Nagappa, Y. R. Kanth, I. G. Lakshmi, and J. B. Rao, "Effect of brachyura shell particles on glass fibre reinforced epoxy polymer composite," *Materials Today: Proceedings*, vol. 42, pp. 555–562, 2020, doi: 10.1016/j.matpr.2020.10.521.
- [71] W. Borja, M. Adarmouch, Y. El Hafiane, Y. Daafi, Y. Tamraoui, and J. Alami, "Synthesis of nano-silica as a promising route of recycling phosphate waste rocks and its incorporation in mortars," *Sustainable Materials and Technologies*, vol. 37, 2023, Art. no. e00684, doi: 10.1016/j.susmat.2023.e00684.
- [72] R. Pramod and V. K. G. Basavaraja, "Investigation of the thermal and mechanical properties of glass fiber reinforced ABS/epoxy blended polymer composite," *Applied Science and Engineering Progress*, vol. 17, no. 4, pp. 1–18, Aug. 2024, doi: 10.14416/j.asep.2024.08.003.